

Analytical results for semiconductor quantum-well wire: Plasmons, shallow impurity states, and mobility

A. Gold

Department of Physics, Massachusetts Institute of Technology, Cambridge, Massachusetts 02139

A. Ghazali

Groupe de Physique des Solides de l'Ecole Normale Supérieure, Université de Paris-VII, 75251 Paris, France

(Received 5 June 1989)

We present a theoretical investigation of the electronic properties of a quasi-one-dimensional electron system at very low temperature. For a cylindrical quantum wire the electron-impurity interaction and the electron-electron interaction is calculated for a two-subband model. Our analytical results for the electron-impurity and the electron-electron interaction are in good agreement with the exact results for our model. Analytical results for the band bending due to the filling of the lowest subband are evaluated. Within our analytical results we discuss various aspects of the electronic properties of the semiconductor quantum wire: screening (intrasubband and intersubband plasmons), shallow impurity states (screened and unscreened), and mobility (ionized-impurity scattering and interface-roughness scattering). Analytical expressions are given for the dispersion of plasmons, the binding energies of shallow impurities, and the mobility. Our results on intersubband plasmons are compared with experiments.

I. INTRODUCTION

Electronic properties of quasi-one-dimensional electron systems (Q1D ES's) have been recently studied experimentally (for a review, see Ref. 1) and theoretically (for a review, see Ref. 2). Usually, quasi-one-dimensional structures are produced by an additional one-dimensional confinement of a two-dimensional electron gas as realized in silicon metal-oxide-semiconductor structures or in $\text{Al}_x\text{Ga}_{1-x}\text{As}/\text{GaAs}$ heterostructures. For realistic calculations of the subband structure in these systems, one must solve a two-dimensional Schrödinger equation and a two-dimensional Poisson equation, and only numerical results are available.³⁻⁵

Analytical results for the subband structure of Q1D ES's can be obtained for a cylinder of radius R_0 with infinite barriers and for a rectangular wire with sides L_1 and L_2 and with infinite barriers. However, even for these models the Fourier transform of the electron-electron interaction potential, which plays a fundamental role for plasmons, has only been given as a numerical result.^{3,6} For the lowest subband and for a cylindrical wire, analytical results for the electron-impurity and electron-electron interaction potentials have been obtained with the approximation of a constant electron density in the wire.^{7,8}

In the past, analytical results for simplified models have been very important for the quantitative understanding of the physics of two-dimensional electron systems. We mention the Howard-Fang variational wave function for silicon metal-oxide-semiconductor (MOS) structures and the $\text{Al}_x\text{Ga}_{1-x}\text{As}/\text{GaAs}$ heterostructures (for a review, see Ref. 9), and the one-dimensional barrier model for quantum wells (for a review, see Ref. 10).

In this paper we present analytical and numerical results for the electron-electron and electron-impurity interaction potentials for the two lowest subbands of a cylindrical wire. The good match of our analytical results with the numerical calculations motivated us to study various electronic properties using our analytical results. We discuss the elementary excitations of the system, the binding energy of shallow impurity states, and the mobility for ionized-impurity and interface-roughness scattering.

Intrasubband plasmons have been studied theoretically in Ref. 11, and numerical results have been given. We present results for a cylindrical symmetry and we discuss various analytical formulas, which are valid for small wave numbers. Our results for intersubband plasmons and the discussion of depolarization effects generalize the well-known results for two-dimensional systems (for a review, see Ref. 9) to Q1D ES's. This calculation is important for the interpretation of infrared experiments.¹

Binding energies of hydrogenic impurities have been calculated within the variational approach.^{12,13} For our calculations we use the separable-potential approximation, which we have successfully used before for the calculation of bound states in two-dimensional electron systems.¹⁴ Bound states for the second subband are also calculated.

Mobility limits for charged-impurity scattering in Q1D ES's have been calculated by Sakaki¹⁵ and later in Refs. 7, 8, and 16 within some more sophisticated models. These calculations will be discussed in the light of our analytical results for the electron-impurity interaction. We also present analytical results for interface-roughness scattering in Q1D ES's.

The paper is organized as follows. In Sec. II we explain the model. Our results for the electron-impurity

and electron-electron interactions are presented in Sec. III. The screening properties of the electron gas and the excitation spectrum are derived in Sec. IV. Shallow impurity states are examined in Sec. V. In Sec. VI we describe the mobility limits of these Q1D ES's. In Sec. VII we discuss the model and compare it with experimental results. We present our conclusions in Sec. VIII.

II. MODEL AND GENERAL FRAMEWORK

In our model the quasi-one-dimensional structure is realized as a circular cylinder of radius R_0 with an infinite potential barrier at $r=R_0$. The motion of electrons is restricted in the $\mathbf{r}=(r, \vartheta)$ plane, while the motion in the z direction is a free motion. An isotropic electron mass m is assumed. The corresponding Schrödinger equation for the motion in the r plane is solved by Bessel functions $J_n(x)$, and the wave function $\phi_{nl}(r, \vartheta)$ inside the wire is expressed as¹⁷

$$\phi_{nl}(r, \vartheta) = \frac{1}{(\pi R_0^2)^{1/2}} \frac{1}{J_{n+1}(\beta_{nl})} J_n(\beta_{nl} r / R_0) e^{\pm i n \vartheta}, \quad (1)$$

with $n=0, 1, 2, \dots$ and $l=1, 2, \dots$. β_{nl} is the l th zero of the Bessel function of order n .¹⁸ Outside the wire the wave function is given by $\phi_{nl}(r > R_0, \vartheta)=0$. The energy eigenvalues are given by

$$E_{nl} = \frac{\hbar^2}{2m} \frac{1}{R_0^2} \beta_{nl}^2, \quad (2)$$

and they define the subband structure in the wire.

In the following we discuss a two-subband model and assume that only the lowest subband is occupied. The two lowest subbands are described by

$$\phi_{01}(r, \vartheta) = \begin{cases} 1.08 J_0(2.40r/R_0)/R_0, & r < R_0 \\ 0, & r \geq R_0 \end{cases} \quad (3a)$$

and

$$\phi_{11}(r, \vartheta) = \begin{cases} 1.40 J_1(3.83r/R_0) e^{\pm i \vartheta} / R_0, & r < R_0 \\ 0, & r \geq R_0 \end{cases} \quad (3b)$$

with energy levels

$$E_{01} = (5.76 \text{ Ry}^*) (a^*/R_0)^2 \quad (4a)$$

and

$$E_{11} = (14.7 \text{ Ry}^*) (a^*/R_0)^2. \quad (4b)$$

In Eqs. (4) we have introduced the effective Rydberg (Ry^*) and the effective Bohr radius ($a^* = \epsilon_L \hbar^2 / m e^2$) via $\hbar^2 / 2m = (1 \text{ Ry}^*) (a^*)^2$ ($\hbar=1$ in the following). ϵ_L is the dielectric constant of the background.

Various electronic properties of the quasi-one-dimensional structure are determined by the electron-impurity and electron-electron interaction potentials. We assume that charged impurities are randomly distributed on the surface of a cylinder with radius R . The interaction between point charges follows the Coulomb law. We introduce the Fourier transform for the z direction with \mathbf{q} as a one-dimensional wave vector. For a system with cylindrical symmetry, the interaction potential between an

electron at \mathbf{r} and an electron at \mathbf{r}' is given by

$$V(\mathbf{r}, \mathbf{r}', \mathbf{q}) = \frac{2e^2}{\epsilon_L} K_0(q|\mathbf{r}-\mathbf{r}'|). \quad (5)$$

K_0 is the modified Bessel function.¹⁸ The effective interactions are weighted with the wave functions. The electron-impurity interaction for an impurity located at $\mathbf{R}=(R, \vartheta)$ is given by

$$V_{ij}^{e-i}(\mathbf{q}, R, \vartheta) = - \int d^2 r' \phi_i^*(\mathbf{r}') \phi_j(\mathbf{r}') V(\mathbf{R}, \mathbf{r}', \mathbf{q}). \quad (6)$$

The electron-electron interaction potential is expressed as

$$V_{ijkl}^{e-e}(\mathbf{q}) = \int d^2 r \int d^2 r' \phi_i^*(\mathbf{r}) \phi_j(\mathbf{r}) V(\mathbf{r}, \mathbf{r}', \mathbf{q}) \phi_k^*(\mathbf{r}') \phi_l(\mathbf{r}'). \quad (7)$$

The electron-impurity interaction potential determines the mobility of the wire for impurity scattering. The electron-electron interaction potential describes the screening properties of the wire.

Our restriction to a two-subband mode ($i=1, 2$) and the cylindrical symmetry implies that only four matrix elements of $V_{ijkl}^{e-e}(\mathbf{q})$ are independent and different from zero: $V_{1111}^{e-e}(\mathbf{q})$, $V_{2222}^{e-e}(\mathbf{q})$, $V_{1221}^{e-e}(\mathbf{q})$, and $V_{1122}^{e-e}(\mathbf{q})$. Moreover, the following relations hold: $V_{1122}^{e-e}(\mathbf{q}) = V_{2211}^{e-e}(\mathbf{q})$, $V_{1221}^{e-e}(\mathbf{q}) = V_{2112}^{e-e}(\mathbf{q}) = V_{1212}^{e-e}(\mathbf{q}) = V_{2121}^{e-e}(\mathbf{q})$. For the electron-impurity interaction potential, one finds $V_{12}^{e-i}(\mathbf{q}, R, \vartheta) = V_{21}^{e-i}(\mathbf{q}, R, -\vartheta)$.

III. ANALYTICAL RESULTS FOR $V^{e-i}(\mathbf{q})$ AND $V^{e-e}(\mathbf{q})$

In this section we calculate the electron-impurity and electron-electron interaction potentials for different approximations of the wave functions.

A. The wave functions

In order to get analytical results for the electron-electron and electron-impurity interaction potentials, we use the following expressions of the normalized wave functions for the two lowest subbands in the infinite-barrier-height approximation:

$$\phi_1(r, \vartheta) = \begin{cases} (3/\pi R_0^2)^{1/2} (1-r^2/R_0^2), & r < R_0 \\ 0, & r \geq R_0 \end{cases} \quad (8a)$$

and

$$\phi_2(r, \vartheta) = \begin{cases} (12/\pi R_0^2)^{1/2} (r/R_0 - r^3/R_0^3) e^{\pm i \vartheta}, & r < R_0 \\ 0, & r \geq R_0. \end{cases} \quad (8b)$$

These simple expressions fulfill the condition that the wave functions vanish at $r=R_0$. The wave functions according to Eqs. (3) and (8) are shown in Fig. 1. Also shown in Fig. 1 is the wave function in the constant-electron-density approximation used in Refs. 7 and 8. From Fig. 1, we conclude that our simple analytical expressions, given in Eqs. (8), are good approximations to

the exact solutions. We mention that the corresponding expectation energies are, respectively, $E_1 = (6 \text{ Ry}^*)(a^*/R_0)^2$ and $E_2 = (16 \text{ Ry}^*)(a^*/R_0)^2$, which are also in good agreement with the exact results; compare with Eqs. (4).

B. The electron-impurity interaction potential

With Eqs. (8) the results for the electron-impurity interaction potential, see Eq. (6), can be obtained in analytical form. We get

$$V_{11}^{e-i}(\mathbf{q}, \mathbf{R}) = -96 \frac{e^2}{\epsilon_L (qR_0)^2} \times \begin{cases} \left[\frac{1}{8} - \frac{1}{4} \left(\frac{R}{R_0} \right)^2 + \frac{1}{8} \left[\left(\frac{R}{R_0} \right)^2 + \frac{8}{(qR_0)^2} \right]^2 - \frac{1}{(qR_0)^2} - \frac{I_0(qR)K_3(qR_0)}{qR_0}, & R < R_0 \\ \frac{K_0(qR)I_3(qR_0)}{qR_0}, & R \geq R_0 \end{cases} \quad (9a)$$

$$V_{12}^{e-i}(\mathbf{q}, \mathbf{R}, \vartheta) = -384 \frac{e^2}{\epsilon_L (qR_0)^2} e^{i\vartheta} \times \begin{cases} \left[\frac{1}{8} \left[1 - \frac{R^2}{R_0^2} \right]^2 \frac{R}{R_0} - \frac{2}{(qR_0)^2} \left[1 - \frac{3R^2}{2R_0^2} \right] \frac{R}{R_0} + 24 \frac{R}{R_0 (qR_0)^4} - \frac{I_1(qR)K_4(qR_0)}{qR_0}, & R < R_0 \\ \frac{K_1(qR)I_4(qR_0)}{qR_0}, & R \geq R_0 \end{cases} \quad (9b)$$

and

$$V_{22}^{e-i}(\mathbf{q}, \mathbf{R}) = -48 \frac{e^2}{\epsilon_L (qR_0)^2} \times \begin{cases} \left[\frac{R}{R_0} - \frac{R^3}{R_0^3} \right]^2 + \frac{4}{(qR_0)^2} \left[1 - 8 \frac{R^2}{R_0^2} + 9 \frac{R^4}{R_0^4} \right] - \frac{128}{(qR_0)^4} \left[1 - \frac{9R^2}{2R_0^2} \right] \\ + \frac{6^2 8^2}{(qR_0)^6} - \frac{8}{qR_0} I_0(qR) \left[K_3(qR_0) + \frac{6}{qR_0} K_4(qR_0) \right], & R < R_0 \\ \frac{8}{qR_0} K_0(qR) \left[I_3(qR_0) - \frac{6}{qR_0} I_4(qR_0) \right], & R \geq R_0. \end{cases} \quad (9c)$$

I_n and K_n are the modified Bessel functions of order n .¹⁸ The following asymptotic results are useful for numerical calculations:

$$V_{11}^{e-i}(qR_0 \ll 1) = \frac{2e^2}{\epsilon_L} \times \begin{cases} \ln \left[\frac{qR_0}{2} \right] - \frac{11}{12} + \mathcal{O} + \frac{3}{2} \left[\frac{R}{R_0} \right]^2 \left[1 - \frac{3}{2} \left[\frac{R}{R_0} \right]^2 + \frac{1}{9} \left[\frac{R}{R_0} \right]^4 \right] + \dots, & R < R_0 \\ -K_0(qR) \left[1 + \frac{q^2 R_0^2}{16} + \frac{q^4 R_0^4}{640} + \dots \right], & R \geq R_0 \end{cases} \quad (10a)$$

and

$$V_{12}^{e-i}(qR_0 \ll 1) = -\frac{e^2}{\epsilon_L} e^{i\vartheta} \times \begin{cases} 4 \frac{R}{R_0} \left[1 - \frac{3}{2} \left[\frac{R}{R_0} \right]^2 + \left[\frac{R}{R_0} \right]^4 - \frac{1}{4} \left[\frac{R}{R_0} \right]^6 + O(q^2) \right], & R < R_0 \\ \frac{R_0}{R} [1 + O(q^2)], & R \geq R_0 \end{cases} \quad (10b)$$

and

$$V_{22}^{e-i}(qR_0 \ll 1) = 2 \frac{e^2}{\epsilon_L} \times \begin{cases} \ln \left[\frac{qR_0}{2} \right] - \frac{13}{24} + \mathcal{O} + \frac{3}{2} \left[\frac{R}{R_0} \right]^4 \left[1 - \frac{8}{9} \left[\frac{R}{R_0} \right]^2 + \frac{1}{4} \left[\frac{R}{R_0} \right]^4 + \dots \right], & R < R_0 \\ -K_0(qR) \left[1 + \frac{q^2 R_0^2}{10} + \frac{q^4 R_0^4}{320} + \dots \right], & R \geq R_0. \end{cases} \quad (10c)$$

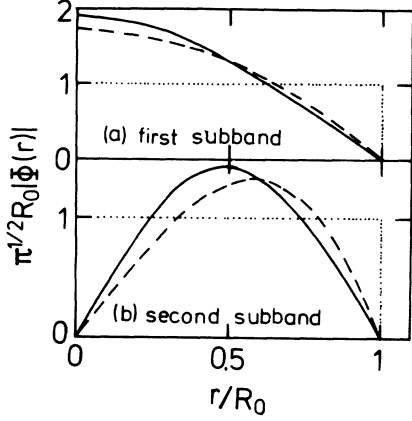


FIG. 1. Wave function (radial part) vs wire radius for the two lowest subbands. The solid lines represent the exact results, see Eq. (3). The dashed lines represent the analytical results, see Eq. (8). The dotted lines represent the approximation used in Refs. 7 and 8.

$\mathcal{C} = 0.577$ is Euler's constant.

$V_{11}^{e-i}(\mathbf{q}, \mathbf{R})$ versus qR_0 is shown in Fig. 2 for $R = 0$. The solid line in Fig. 2(a) is the exact result according to Eqs. (3a) and (6). The dashed line is the analytical result according to Eq. (9a). The dotted line is the analytical result of Fishman;⁷ however, see Ref. 19. It is clearly seen that our analytical result is in very good agreement with the numerical result. The solid lines in Fig. 2(b) show the analytical result according to Eq. (9a) for various values of R . With increasing distance of the impurities from the center of the wire, the electron-impurity interaction potential decreases.

In Figs. 3(a) and 3(b) we show $V_{12}^{e-i}(\mathbf{q}, \mathbf{R})$ and $V_{22}^{e-i}(\mathbf{q}, \mathbf{R})$, respectively, versus qR_0 for various values of R . The solid lines are the numerical results according to Eqs. (3) and (6). The dashed lines are the analytical results according to Eqs. (9). Again, we find very good agreement between the numerical results and our analyti-

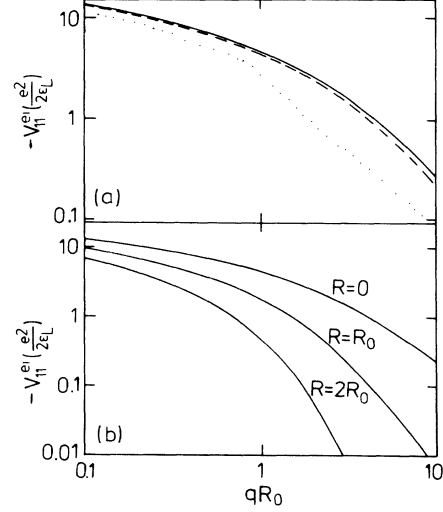


FIG. 2. Electron-impurity interaction potential V_{11}^{e-i} vs wave number (a) For $R = 0$. The solid, dashed, and dotted lines correspond to Eq. (6) (exact result), Eq. (9a) (analytical result), and the analytical result of Ref. 7, respectively. (b) For $R = 0, R_0$, and $2R_0$. The solid lines represent the analytical result, see Eq. (9a).

cal calculations. We mention that $V_{11}^{e-i}(\mathbf{q}, \mathbf{R})$ and $V_{22}^{e-i}(\mathbf{q}, \mathbf{R})$ have the characteristic logarithmic singularity $\ln(qR_0/2)$ for $qR_0 \ll 1$; however, this is not the case for $V_{12}^{e-i}(\mathbf{q}, \mathbf{R})$. $V_{12}^{e-i}(\mathbf{q}, \mathbf{R} = 0)$ is zero and is not shown in Fig. 3(a), see Eq. (10b).

In the following subsections we will use the analytical results for the calculation of the binding energy of shallow impurity states and the mobility.

C. The electron-electron interaction potential

With Eqs. (8) the results for the electron-electron interaction potential, see Eq. (7), can be given in analytical form. We get

$$V_{1111}^{e-e}(\mathbf{q}) = 72 \frac{e^2}{\epsilon_L (qR_0)^2} \left[\frac{1}{10} - \frac{2}{3(qR_0)^2} + \frac{32}{3(qR_0)^4} - \frac{64}{(qR_0)^4} I_3(qR_0) K_3(qR_0) \right], \quad (11a)$$

$$V_{1122}^{e-e}(\mathbf{q}) = 288 \frac{e^2}{\epsilon_L (qR_0)^2} \left[\frac{1}{60} - \frac{1}{15(qR_0)^2} + \frac{8}{3(qR_0)^4} - \frac{64}{(qR_0)^4} K_3(qR_0) \left[I_3(qR_0) - \frac{6}{qR_0} I_4(qR_0) \right] \right], \quad (11b)$$

$$V_{1221}^{e-e}(\mathbf{q}) = 576 \frac{e^2}{\epsilon_L (qR_0)^2} \left[\frac{1}{60} - \frac{4}{15(qR_0)^2} + \frac{8}{(qR_0)^4} - \frac{64}{(qR_0)^4} I_4(qR_0) K_4(qR_0) \right], \quad (11c)$$

and

$$V_{2222}^{e-e}(\mathbf{q}) = 1152 \frac{e^2}{\epsilon_L (qR_0)^2} \left[\frac{1}{210} - \frac{1}{15(qR_0)^2} + \frac{64}{15(qR_0)^4} + \frac{96}{(qR_0)^6} - \frac{64}{(qR_0)^4} \left[I_3(qR_0) - \frac{6}{qR_0} I_4(qR_0) \right] \left[K_3(qR_0) + \frac{6}{qR_0} K_4(qR_0) \right] \right]. \quad (11d)$$

Asymptotic results are expressed as

$$V_{1111}^{e-e}(qR_0 \ll 1) = -2 \frac{e^2}{\epsilon_L} \left[\ln \left[\frac{qR_0}{2} \right] \left[1 + \frac{1}{8}(qR_0)^2 + \frac{9}{2^8 5}(qR_0)^4 + \frac{11}{2^{10} 3^2 5}(qR_0)^6 + \dots \right] \right. \\ \left. - \frac{73}{120} + \mathcal{C} - \frac{1}{8}(qR_0)^2 \left(\frac{1949}{1680} - \mathcal{C} \right) - \frac{1}{2^8 5}(qR_0)^4 \left(\frac{10673}{280} - 9\mathcal{C} \right) + \dots \right], \quad (12a)$$

$$V_{1122}^{e-e}(qR_0 \ll 1) = -2 \frac{e^2}{\epsilon_L} \left[\ln \left[\frac{qR_0}{2} \right] [1 + O(q^2)] + O(q^0) \right], \quad (12b)$$

$$V_{1221}^{e-e}(qR_0 \ll 1) = \frac{8e^2}{7\epsilon_L} [1 - O(q^2)], \quad (12c)$$

and

$$V_{2222}^{e-e}(qR_0 \ll 1) = -2 \frac{e^2}{\epsilon_L} \left[\ln \left[\frac{qR_0}{2} \right] [1 + \frac{1}{5}(qR_0)^2 + \dots] + \mathcal{C} - \frac{617}{1680} - (qR_0)^2 \left(\frac{247}{3360} - \mathcal{C}/5 \right) + \dots \right]. \quad (12d)$$

$V_{1111}^{e-e}(\mathbf{q})$ versus qR_0 is shown in Fig. 4. The solid line is the numerical result according to Eqs. (3a) and (7). The dashed line is the analytical result, see Eq. (11a). The dashed-dotted line is the analytical result of Refs. 7 and 8. The dotted line is the asymptotic law for $qR_0 \ll 1$, see Eq. (12a). From Eq. (11a) we get, for $qR_0 \gg 1$,

$$V_{1111}^{e-e}(qR_0 \gg 1) = \frac{72e^2}{\epsilon_L (qR_0)^2} \left[\frac{1}{10} - \frac{2}{3(qR_0)^2} + \frac{32}{3(qR_0)^4} \right]. \quad (13)$$

We mention the good agreement between the exact result and our analytical result. The asymptotic law, see Eq. (12a), is a very good approximation for $qR_0 < 1$. The solid circles in Fig. 4 are numerical results for a square wire.⁶ We used the relation $L^2 = \pi R_0^2$ to scale the side L of the wire to the radius R_0 .

$V_{1122}^{e-e}(\mathbf{q})$ and $V_{1221}^{e-e}(\mathbf{q})$ versus qR_0 are shown in Figs. 5(a) and 5(b), respectively. The numerical results (solid lines) are again in very good agreement with our analytical results. We mention that V_{1111}^{e-e} , V_{1122}^{e-e} , and V_{2222}^{e-e} show the characteristic $\ln(qR_0)$ (singular) behavior for

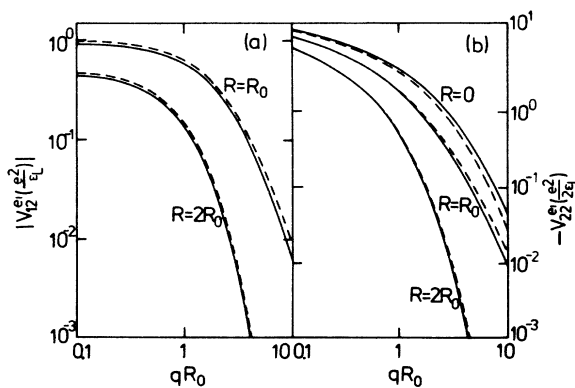


FIG. 3. Electron-impurity interaction potential vs wave number: (a) V_{12}^{e-i} and (b) V_{22}^{e-i} . The solid and dashed lines represent the exact result, see Eq. (6), and the analytical result, see Eqs. (9b) and (9c), respectively.

$qR_0 \ll 1$. However, V_{1221}^{e-e} becomes constant for $qR_0 \ll 0$. The result for V_{1111}^{e-e} is very important for the intrasubband plasmon excitations of the system, while V_{1221}^{e-e} determines the depolarization-shifted intersubband resonance. These two results will be discussed in Sec. IV. The symmetry relations for V_{ijkl}^{e-e} have been given in Sec. II.

In Fig. 6 we show $V_{2222}^{e-e}(\mathbf{q})$ versus qR_0 . The solid line is the numerical result according to Eqs. (3b) and (7), the dashed line is our analytical result according to Eq. (11d), and the dotted line is the asymptotic law for $qR_0 \ll 1$, see Eq. (12d).

D. The band bending

Our preceding discussion was restricted to a Q1D ES confined by an external potential barrier. The filling of the subbands introduces an additional potential which can be approximated as a Hartree term. If we assume that only the lowest subband is occupied by electrons, the

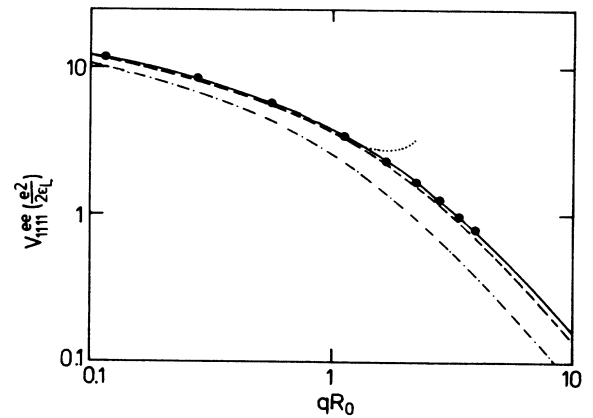


FIG. 4. Electron-electron interaction potential V_{1111}^{e-e} vs wave number. The solid and dashed lines correspond to Eqs. (7) (exact result) and (11a) (analytical result), respectively. The dashed-dotted line refers to Refs. 7 and 8. The dotted line is for $qR_0 \ll 1$, see Eq. (12a). The solid circles represent numerical results for a square wire (Ref. 6), see text.

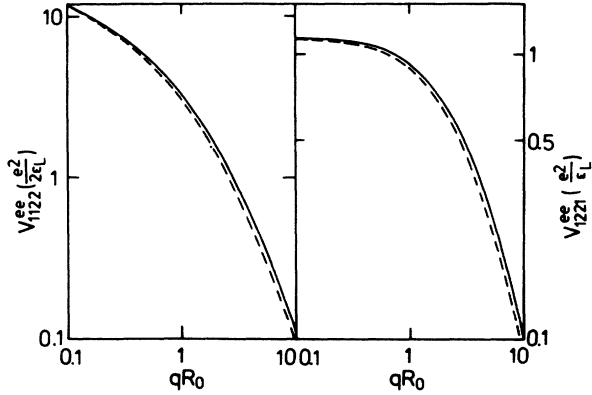


FIG. 5. Electron-electron interaction potential vs wave number: (a) V_{1122}^{ee} and (b) V_{1221}^{ee} . The solid and dashed lines represent the exact results, see Eq. (7), and the analytical results, see Eqs. (11b) and (11c), respectively.

finite electron density gives rise to a potential $\Sigma(r)$, which can be calculated by the Poisson equation:

$$\frac{d^2}{dr^2} \Sigma(r) + \frac{1}{r} \frac{d}{dr} \Sigma(r) = -\frac{4\pi e^2 N}{\epsilon_L} |\phi_1(r)|^2. \quad (14)$$

N is the one-dimensional electron density. With Eq. (8a) we get

$$\Sigma(r) = \frac{A}{4} \left[\frac{11}{18} - \left(\frac{r}{R_0} \right)^2 + \frac{1}{2} \left(\frac{r}{R_0} \right)^4 - \frac{1}{9} \left(\frac{r}{R_0} \right)^6 \right] \quad (15a)$$

and

$$A = \frac{12e^2 N}{\epsilon_L} = (24 \text{ Ry}^*) Na^* . \quad (15b)$$

The potential $\Sigma(r)$ gives rise to a band bending, and this is schematically shown in Fig. 7. The shift of the energy levels, ΔE_i , due to this potential can be calculated in perturbation theory, and, with Eqs. (8) and (15), we get, to first order,

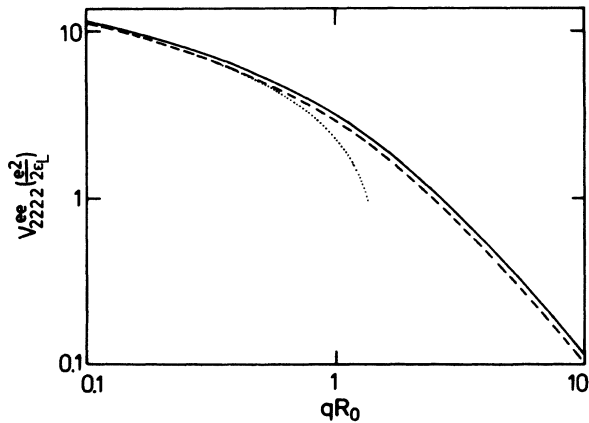


FIG. 6. Electron-electron interaction potential V_{2222}^{ee} vs wave number. The solid and dashed lines represent the exact result, see Eq. (7), and the analytical result, see Eq. (11d), respectively. The dotted line is for $qR_0 \ll 1$, see Eq. (12d).

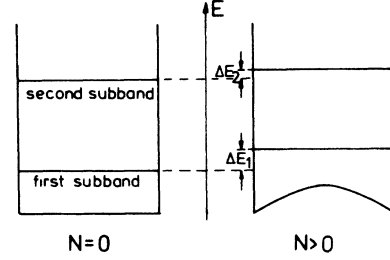


FIG. 7. Band bending in quantum wires: influence of a finite electron density on the subband energies, see Eqs. (16).

$$\Delta E_1 = \frac{73}{2^4 3^2 5} A \approx (2.4 \text{ Ry}^*) Na^* \quad (16a)$$

and

$$\Delta E_2 = \frac{47}{3^2 70} A \approx (1.8 \text{ Ry}^*) Na^* . \quad (16b)$$

According to Eqs. (16), we expect a decrease of the intersubband energy separation with increasing electron density, see Fig. 7. However, in our model we assumed that the effective width of the wire does not depend on the electron density. In the structures used in experiments, usually the confinement depends on the electron density, and an additional dependence of the intersubband energy on the electron density is expected. This effect could be qualitatively modeled by a density dependence of $R_0 = R_0(N)$.

In this section the band bending due to a finite electron density has been calculated. An overall charge neutrality has been assumed. In principle, one should also consider the effects of donor atoms which we have neglected.

IV. PLASMONS

As the first application of our calculated electron-electron interaction potentials, we discuss in this section the collective excitation spectrum for the Q1D ES's.

A. General results

The dielectric tensor of a multisubband system is defined by⁹

$$\epsilon_{ijmn}(\mathbf{q}, \Omega) = \delta_{ij} \delta_{mn} + X_{ij}(\mathbf{q}, \Omega) V_{ijmn}^{e-e}(\mathbf{q}) . \quad (17)$$

$X_{ij}(\mathbf{q}, \Omega)$ is the generalized Lindhard function for wave vector \mathbf{q} and frequency Ω . δ_{ij} is the Kronecker symbol. We restrict our discussion to a two-subband model, where only the lowest subband is occupied by electrons. The collective modes for this model are given by

$$[1 + V_{1111}^{e-e}(\mathbf{q}) X_{11}(\mathbf{q}, \Omega)][1 + V_{1221}^{e-e}(\mathbf{q}) X_{12}(\mathbf{q}, \Omega)] = 0 . \quad (18)$$

A similar model has been discussed for two-dimensional systems.²⁰ From Eq. (18) it is clear that in our two-subband model two collective modes are present. The first collective mode is the intrasubband plasmon, given by²¹

$$1 + V_{1111}^{e-e}(\mathbf{q})X_{11}(\mathbf{q}, \Omega) = 0, \quad (19a)$$

and the second collective mode is the intersubband plasmon,

$$1 + V_{1221}^{e-e}(\mathbf{q})X_{12}(\mathbf{q}, \Omega) = 0. \quad (19b)$$

B. The intrasubband plasmons

Intrasubband plasmons for one-dimensional systems have been discussed in Refs. 22–24 and recently in Ref. 11. In the following we present some analytical results for the intrasubband plasmons. The Lindhard function $X_{11}(\mathbf{q}, \Omega)$ for one-dimensional systems is expressed as²³

$$X_{11}(\mathbf{q}, \Omega) = \frac{m}{\pi q} \left[\ln \left| \frac{\Omega^2 - \Omega_+^2}{\Omega^2 - \Omega_-^2} \right| + i\pi \Theta(\Omega_+ - \Omega) \Theta(\Omega - \Omega_-) \right] \quad (20)$$

and

$$\Omega_{\pm} = |q^2 \pm 2qk_F| / 2m. \quad (21)$$

$\Theta(x)$ is the unit-step function. k_F is the Fermi wave number. The real part of $X_{11}(\mathbf{q}, \Omega)$ determines the plasmon dispersion, while the imaginary part determines the particle-hole excitation spectrum.²¹

In Fig. 8 we show the intrasubband plasmon energy versus q (solid line) according to Eq. (19a) and the particle-hole excitation spectrum versus q (hatched area). Analytical results for the plasmon dispersion can be derived as follows. The large frequency expansion of the Lindhard function for Q1D ES's is expressed as

$$-X_{11}(\mathbf{q}, \Omega) = \frac{N}{m} \frac{q^2}{\Omega^2} \left[1 + \frac{f_1(q)}{\Omega^2} + O\left(\frac{1}{\Omega^4}\right) \right] \quad (22a)$$

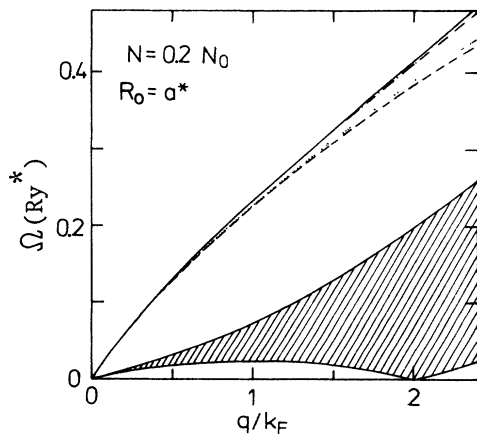


FIG. 8. Excitation spectrum of a quantum wire. The hatched area indicates the particle-hole spectrum. The solid line represents the intrasubband plasmon, calculated according to Eq. (19a). The dashed, dashed-dotted, and dotted lines represent Eqs. (23), (24a), and (24b), respectively.

and

$$f_1(q) = q^2(q^2 + 4k_F^2) / 4m^2. \quad (22b)$$

With $V_{1111}^{e-e}(\mathbf{q}) \approx -2e^2 \ln(qR_0/2) / \epsilon_L$ for $qR_0 \ll 1$, we get, with Eqs. (19a) and (22a),

$$\Omega(qR_0 \ll 1) / \Omega_0 = qR_0 [\ln(2/qR_0)]^{1/2} \quad (23a)$$

and

$$\Omega_0^2 = 2Ne^2 / \epsilon_L mR_0^2. \quad (23b)$$

The dashed line in Fig. 8 corresponds to Eq. (23). With $V_{1111}^{e-e}(\mathbf{q}) = e^2 f(q) / 2\epsilon_L$, we get, with Eqs. (19a) and (22a),

$$\Omega(qR_0 \ll 1) / \Omega_0 = qR_0 \left\{ \frac{f(q)}{2} \left[1 + \left[1 + 4 \frac{f_1(q)}{\Omega_0^2 f(q) (qR_0)^2} \right]^{1/2} \right] \right\}^{1/2}, \quad (24a)$$

which corresponds to the dashed-dotted line in Fig. 8. The dotted line corresponds to Eq. (24a) with $f_1(q) = 0$:

$$\Omega(qR_0 \ll 1) / \Omega_0 = qR_0 [f(q)]^{1/2}. \quad (24b)$$

It can be seen from Fig. 8 that our simplest expression for the plasmon frequency, see Eq. (23a), is a very good approximation to the full solution for $q < k_F$. For higher q , nonlocal effects [$f_1(q)$] in the dispersion relation become important, and our analytical result [Eq. (24a)] is in very good agreement with the exact calculation for $q < 2k_F$.

In Ref. 11 it was argued that asymptotic results for $qR_0 \ll 1$ have a very small range of validity. The discrepancy between our results and those of Ref. 11 emerges from the fact that in Ref. 11 the factor 2 in Eq. (23a) was neglected. The plasmon frequency in Q1D ES's depends on the confinement (R_0), see Eqs. (23). This dependence could be used to get information about R_0 .

For a different model the effects of local-field corrections on the plasmon dispersion have been discussed.²⁴ We have neglected these effects because our main aim was the presentation of the analytical results. However, local-field effects, described by $G(\mathbf{q})$, could be easily incorporated in our analytical results: One has to replace $f(q)$ in Eqs. (24) by $f(q)[1 - G(\mathbf{q})]$. In Eq. (19a), $V_{1111}^{e-e}(\mathbf{q})$ has to be replaced by $V_{1111}^{e-e}(\mathbf{q})[1 - G(\mathbf{q})]$. Analytical results for $G(\mathbf{q})$ are easily obtained in Hubbard's approximation. We follow the derivation of Singwi *et al.*²⁵ for three-dimensional systems and find, for Q1D ES's,

$$G_H(\mathbf{q}) = \frac{1}{2g_v} \frac{V_{1111}^{e-e} [(q^2 + k_F^2)^{1/2}]}{V_{1111}^{e-e}(\mathbf{q})}. \quad (25)$$

g_v is the valley degeneracy. The effect of Hubbard's local-field correction on the intrasubband plasmon is shown in Fig. 9. It indicates that local-field corrections have a significant effect on the plasmon dispersion, and a more sophisticated theory²⁴ should be used to get quantitative results. However, local-field effects become smaller for larger electron density, see Eq. (25). The analytical

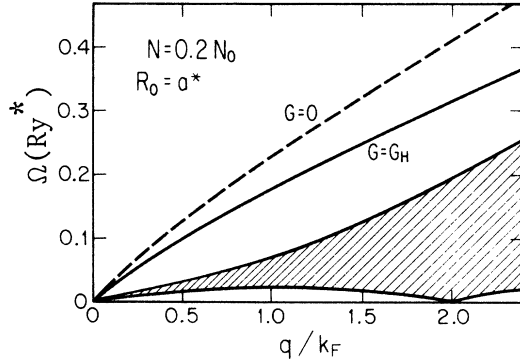


FIG. 9. Excitation spectrum of a quantum wire. The hatched area indicates the particle-hole spectrum. The solid and dashed lines represent the intrasubband plasmon in the random-phase approximation with and without local-field corrections [in Hubbard's approximation, see Eq. (25)], respectively.

result for $G_H(\mathbf{q})$ gives at least a rough estimate of the correction to the random-phase approximation.

C. The intersubband plasmons

For $qR_0 \ll 1$ the off-diagonal polarizability is given by

$$-X_{12}(qR_0 \ll 1, \Omega) = 2N \frac{E_{21}}{\Omega^2 - E_{21}^2}, \quad (26)$$

and $E_{21} = E_2 - E_1$ is the subband distance. This result does not depend on the dimension of the system and also holds for two-dimensional systems.²⁶ With Eqs. (12c) and (19b), we get

$$\Omega(q=0) = (E_{21}^2 + \Omega_{dp}^2)^{1/2} \quad (27a)$$

and

$$\Omega_{dp}^2 = 2NE_{21} V_{1221}^{e-e}(\mathbf{q}=\mathbf{0}) = \frac{32}{7} Na^* E_{21} (1 \text{ Ry}^*). \quad (27b)$$

Ω_{dp} is the depolarization shift, well known for two-dimensional systems.^{26,27} Recently, the depolarization-shifted intersubband resonance in multiwire superlattices has been calculated²⁸ and measured.²⁹ In two-dimensional systems a mode-coupling effect between intrasubband and intersubband plasmons has been discussed.²⁰ This effect is not present in our model because $V_{1112}^{e-e}(\mathbf{q})=0$.

$$\begin{aligned} (\epsilon_B)^{1/2} = & 24\pi C(1) \{ 48[H_2(u) - Y_2(u)]/u^4 + 8(1 - 36/u^2)[H_3(u) - Y_3(u)]/u^3 \\ & - 96/105\pi u + 8(1 + 32/u^2 + 576/u^4)/\pi u^4 \}. \end{aligned} \quad (31b)$$

The asymptotic solution of Eqs. (31) for $u \ll 1$ is given by

$$(\epsilon_B)^{1/2} = -2C(1) \ln(u/2). \quad (32)$$

The binding energy versus R_0 is shown in Fig. 10 for the first (solid line) and second subbands (dashed line).

V. SHALLOW IMPURITY STATES

A. The separable-potential approximation

In the separable-potential approximation the electron-impurity interaction potential is written as

$$V_{ii}^{e-i}(\mathbf{q}-\mathbf{q}') = C(d) [V_{ii}^{e-i}(\mathbf{q})]^{1/2} [V_{ii}^{e-i}(\mathbf{q}')]^{1/2}. \quad (28)$$

$C(d)$ is a numerical coefficient that depends on the dimensionality d of the system. The binding energy E_B for shallow impurities and $d=1$ is given by the solution of the following equation:

$$\frac{C(1)}{2\pi} \int_{-\infty}^{\infty} d\mathbf{q} \frac{V_{ii}^{e-i}(\mathbf{q})}{\epsilon(\mathbf{q})} \frac{1}{E_B + q^2/2m} = -1. \quad (29)$$

For the first and second subbands, we use $V_{ii}^{e-i}(\mathbf{q}) = V_{11}^{e-i}(\mathbf{q})$ and $V_{ii}^{e-i}(\mathbf{q}) = V_{22}^{e-i}(\mathbf{q})$, respectively. In the following we will discuss unscreened impurities [$\epsilon(\mathbf{q})=1$] and screened impurities. For screened impurities we use $\epsilon(\mathbf{q}) = \epsilon_{1111}(\mathbf{q})$ for the first subband and $\epsilon(\mathbf{q}) = \epsilon_{2222}(\mathbf{q})$ for the second subband, see Eq. (17).

The coefficient $C(3)$ was determined in Ref. 30 from the binding energy of an unscreened Coulomb potential: $C(3) = \frac{1}{2}$. For an ideally two-dimensional system, we used the exact result that $E_B = 4 \text{ Ry}^*$: $C(2) = 2/\pi$.¹⁴ An exactly solvable Coulomb model is not available in one dimension. For this reason we used the variational result of Bryant¹² to specify $C(1)$. In Ref. 12 the binding energy for an impurity located in the center of the wire with radius $R_0 = 0.56a^*$ was given: $E_B = 5 \text{ Ry}^*$. With Eqs. (9a) and (29) we find

$$C(1) = 0.90. \quad (30)$$

B. Unscreened shallow impurities

For impurities located in the center of the wire ($R=0$), analytical results for the binding energy can be obtained. With Eqs. (9a) and (29) we get, for the lowest subband,

$$\begin{aligned} (\epsilon_B)^{1/2} = & 6\pi C(1) \{ 8[H_3(u) - Y_3(u)]/u^3 \\ & - 2(1 + 8/u^2 + 64/u^4)/\pi u^2 \}, \end{aligned} \quad (31a)$$

with $\epsilon_B = E_B/(1 \text{ Ry}^*)$ and $u = \epsilon_B^{1/2} R_0/a^*$. $H_n(u)$ is the Struve function and $Y_n(u)$ is the modified Bessel function of order n .¹⁸ For the second subband we get, with Eq. (9c),

The dotted line is the asymptotic result for $u \ll 1$, see Eq. (32), and is a good approximation to the exact solutions only for very thin wires. The solid circles in Fig. 10 are theoretical results from Ref. 12, where a variational approach was used. As seen, these results agree very well with ours. The decrease of the binding energy with in-

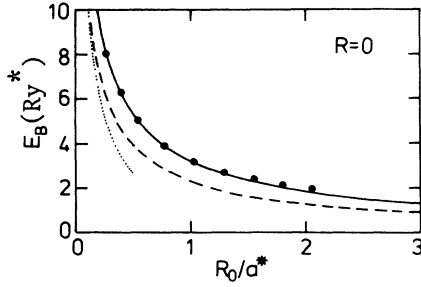


FIG. 10. Binding energy vs wire radius for impurities located in the center of the wire. The solid and dashed lines represent Eqs. (31a) and (31b) for the first and second subbands, respectively. The dotted line is the asymptotic result, see Eq. (32). The solid circles represent variational results for the lowest subband from Ref. 12.

creasing wire radius has also been found within the variational approach in Refs. 31–34.

In Fig. 11 we show the binding energy versus R_0 for the first subband and for various positions of the impurities. With increasing wire radius, the binding energy decreases.^{31,33,34} From Fig. 11 we conclude that the binding energy approximately follows the law

$$E_B \propto (a^*/R_0)^\beta, \quad (33)$$

with $\beta=0.8, 0.85,$ and 0.90 for $R=0, R_0,$ and $2R_0,$ respectively. For very small wire radius our model becomes unrealistic, because we neglected the penetration effects due to the infinite-barrier approximation.

In Fig. 12 the binding energy versus the position of impurities is shown for various values of R_0 . The solid and dashed lines represent the results for the first and second subbands, respectively. For $R \ll R_0$ the binding energy is nearly independent of R [for the second subband (dashed lines) the binding energy increases very slightly with increasing R], and decreases with increasing R for $R > R_0$. For $R > R_0$ we find the approximate result

$$E_B \propto (R/R_0)^{-1}, \quad (34)$$

and we did not find a significant difference in E_B for the first and second subbands. As in two-dimensional systems, the strong dependence of E_B on the position of the

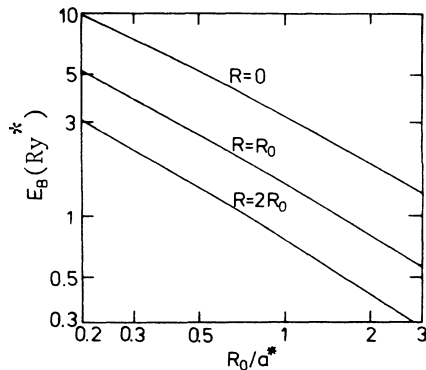


FIG. 11. Binding energy vs wire radius for the first subband and for different impurity positions.

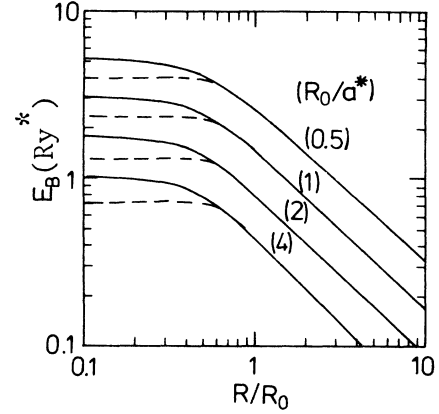


FIG. 12. Binding energy vs impurity position for different wire radii for the first (solid lines) and second subbands (dashed lines).

impurities, see Figs. 11 and 12, may lead to a broad density of states for a spread doping, see, e.g., Ref. 34.

For the calculation of E_B for the second subband, we used Eq. (29) with $V_{ii}^{e-i}(\mathbf{q})=V_{22}^{e-i}(\mathbf{q})$ with $\epsilon(\mathbf{q})=1$. So we neglected the interaction with the continuum of the first-subband states. For two-dimensional systems it has been shown³⁵ that this is a very good approximation, and we expect the same result for Q1D ES's.

The qualitative behavior of E_B versus R_0 and versus R reflects the dependence of the electron-impurity interaction potential on R_0 and R , see Fig. 2. A weak dependence of E_B on the subband index for $R > R_0$ has been found for two-dimensional systems.³⁶ For $R > R_0$ the main contribution to the integral in Eq. (29) comes from $qR_0 \ll 1$, see Figs. 2 and 3, but for $qR_0 \ll 1$ the electron-impurity interaction potential is given by $V_{nn}^{e-i}(qR_0 \ll 1) \approx e^2 \ln(qR_0/2)/2\epsilon_L$ and does not depend on the subband index n .

C. Screened shallow impurities

The binding energy of shallow impurities in two-dimensional systems is strongly reduced by screening via unbound carriers,^{37,38} eventually due to a nonvanishing compensation. This behavior has been confirmed in the separable-potential approximation.¹⁴ With increasing electron density, the binding energy decreases and approaches a constant for large electron density.

For Q1D ES's the screening effect on the binding energy of shallow impurity states has been calculated recently.⁶ With increasing electron density, the binding energy first decreases and later increases again.

The binding energy versus electron density is shown in Fig. 13 for the first subband and for an impurity located in the center of the wire. The relevant static dielectric function, see Eqs. (17) and (20), has been used in Eq. (29). In Ref. 6 a wire with a square cross section and side measuring $L=1.5a^*$ has been considered. The variational results of Ref. 6 are shown in Fig. 13 as solid circles. We use $L^2=\pi R_0^2$, which corresponds to $R_0=0.85a^*$ for $L=1.5a^*$, to compare our results with those of Ref. 6. However, we have to mention that the theoretical results

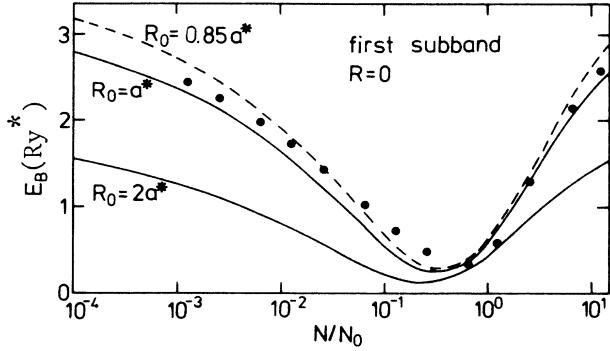


FIG. 13. Binding energy vs electron density in units of $N_0 = 1/2a^*$ according to Eq. (29) for the first subband and for different wire radii. The solid dots represent variational results from Fig. 2 of Ref. 6 for $R_0 = 0.85a^*$, see text.

in Figs. 1(c) and 2 of Ref. 2 seem to be inconsistent. We used the result shown in Fig. 2 of Ref. 6 in our Fig. 13. We find that the minimum of E_B versus N at $N = N^*$ shifts to lower N with increasing R_0 , in agreement with the results given in Ref. 6.

The results for E_B versus N for the second subband are shown in Fig. 14. Behavior similar to that of the first subband is found. The binding energies for the second subband are smaller than for the first subband; also see Fig. 12.

For $d = 3$ it is well known that for large electron density the bound state disappears ($E_B = 0$). In two-dimensional systems E_B becomes constant for large electron density, and finally in Q1D ES's the binding energy has a minimum at $N = N^*$ and increases again for $N > N^*$.

VI. MOBILITY

A. General results

A general expression of the mobility of the d -dimensional interacting-electron gas in the presence of disorder was derived in Ref. 39. According to this theory, the inverse momentum-relaxation time for zero frequency, zero temperature, and for the lowest subband is given by

$$\frac{1}{\tau(\Omega=0)} = \frac{1}{dmN} \sum_q q^2 \frac{\langle |U(\mathbf{q})|^2 \rangle}{[\epsilon(\mathbf{q})]^2} \phi_{\text{FG}}(\mathbf{q}, \Omega=0)'' . \quad (35)$$

$$\epsilon(q = 2k_F, T \ll \epsilon_F) = 1 + \frac{g_v}{\pi} \frac{2\epsilon_L}{e^2} \frac{V_{1111}^{e-e}(2k_F)}{2k_F a^*} [1 - G(2k_F)] \ln \left[\frac{2^3 e^c \epsilon_F}{\pi k_B T} \right] . \quad (39)$$

k_B is the Boltzmann constant. In Eq. (39) we have introduced the local-field correction. Local-field corrections have not been discussed in Refs. 7, 8, and 40. For the calculations, we used Hubbard's approximation, see Eq. (25).

Equations (37)–(39) define the mobility of Q1D ES's in the lowest-order Born approximation for an unspecified random potential. In the following we discuss the mobili-

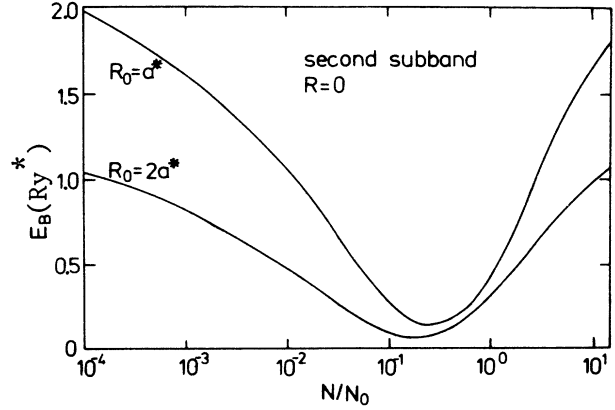


FIG. 14. Binding energy vs electron density in units of $N_0 = 1/2a^*$ according to Eq. (29) for the second subband and for different wire radii.

$\langle |U(\mathbf{q})|^2 \rangle$ is the averaged squared Fourier transform of the random potential and is specified later. $\phi_{\text{FG}}(\mathbf{q}, \Omega)$ is the density-density relaxation function of the noninteracting-electron gas (FG means free gas). $\epsilon(\mathbf{q})$ is the dielectric function for the lowest subband: $\epsilon(\mathbf{q}) = \epsilon_{1111}(\mathbf{q})$. Electron-electron interaction effects within the random-phase approximation are included in Eq. (35) via the dielectric function. For one-dimensional systems, we use the results of Ref. 23 to get

$$\phi_{\text{FG}}(\mathbf{q}, \Omega=0)'' = 2\pi\rho_F m k_F [\delta(2k_F - q)]/q^2 . \quad (36)$$

ρ_F is the density of states of the free-electron gas at the Fermi energy ϵ_F : $\rho_F = 2g_v m / \pi k_F$. From Eqs. (35) and (36) we find

$$\frac{1}{\tau(0)} = \frac{k_F}{\epsilon_F} \frac{\langle |U(2k_F)|^2 \rangle}{\epsilon(2k_F)^2} . \quad (37)$$

The relaxation time determines the mobility μ via

$$\mu = e\tau(0)/m . \quad (38)$$

For one-dimensional systems, $\epsilon(q, T)$ diverges for $q = 2k_F$ and temperature $T = 0$. According to Eqs. (37) and (38), the mobility would go to infinity. However, at finite temperature T , $\epsilon(q = 2k_F, T > 0)$ is finite and can be expressed by^{7,8,40}

ty limits for remote-impurity scattering, homogeneous-background scattering, and interface-roughness scattering. It is well known that for one-dimensional electron systems localization effects are expected to be very important; for a review, see Ref. 41. However, we believe that for finite temperature and weak disorder our results could at least be used to estimate the mobility. We mention that the mobility in one-dimensional systems is expected

to be temperature dependent in the Born approximation. Effects of disorder on the polarizability will weaken this temperature dependence.¹¹

The effect of local-field corrections on the mobility of Q1D ES's is calculated for the first time in this paper. We shall see that the mobility is considerably reduced due to local-field corrections.

B. Remote-impurity doping

Scattering by remote impurities is defined as follows: Impurities are randomly distributed on a cylinder with radius R . The random potential for remote doping (RD) is expressed as

$$\langle |[U(\mathbf{q})]_{\text{RD}}|^2 \rangle = N_i [V_{11}^{e-i}(\mathbf{q})]^2. \quad (40)$$

N_i is the (one-dimensional) impurity density. The mobility is given by

$$\mu_{\text{RD}} = \frac{\pi}{g_v} \frac{e}{\hbar} (a^*)^2 \frac{N}{N_i} \left[\frac{e^2}{2\epsilon_L} \right]^2 \frac{[\epsilon(2k_F, T)]^2}{[V_{11}^{e-i}(2k_F)]^2}. \quad (41)$$

For a GaAs wire with $a^* = 100 \text{ \AA}$ and $g_v = 1$, the prefactor in Eq. (41) becomes $\pi e (a^*)^2 / \hbar = 4.78 \times 10^3 \text{ cm}^2/\text{V s}$.

The mobility for remote-impurity doping versus electron density is shown in Fig. 15. The impurity density is fixed at $N_i = 1 \times 10^6 \text{ cm}^{-1}$. For uncompensated semiconductors, one expects, because of charge neutrality, $N = N_i$. With $\mu \propto 1/N_i$ one can rescale the mobility. With increasing electron density the mobility increases due to the weaker electron-impurity interaction, see Fig. 2(a). With increasing R the density dependence of the mobility increases due to the strong decrease of the electron-impurity interaction potential, see Fig. 2(b).

For the solid lines in Fig. 15, Hubbard's local-field correction to the random-phase approximation has been included, while for the dashed lines it is absent. Local-field effects are most important for the small electron densities: for $N = 1 \times 10^5 \text{ cm}^{-1}$ the local-field effect reduces the mobility by a factor of about 3.

Our calculated mobility is smaller [even for $G(q) = 0$] than the mobility calculated in Refs. 7 and 8. This is due to our larger electron-impurity interaction potential, and the difference is larger for higher electron densities, see Fig. 2(a).

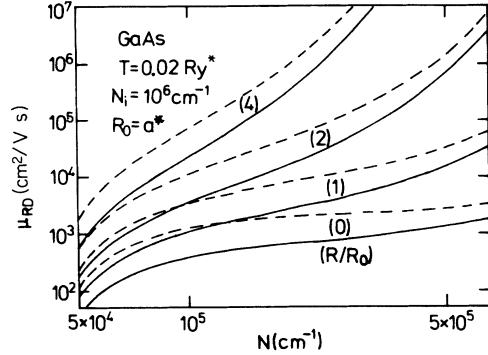


FIG. 15. Mobility for remote doping vs electron density for a GaAs quantum wire, see Eq. (41). The solid (dashed) lines represent calculations with (without) local-field corrections to the random-phase approximation [see Eq. (25)].

Very recently, numerical results for the mobility of Q1D ES's for impurity scattering have been presented in Ref. 42. However, within the harmonic-oscillator model analytical results have not been derived in Ref. 42.

C. Homogeneous-background doping

For homogeneous-background (B) doping, we consider two models. For model 1 ($B1$), impurities are homogeneously distributed in the wire ($0 < R < R_0$). The (three-dimensional) impurity density is N_{B1} . For model 2 ($B2$), the impurities are homogeneously distributed outside of the wire ($R > R_0$). The (three-dimensional) impurity density is N_{B2} . The random potential is defined as

$$\langle |[U(\mathbf{q})]_{B1(B2)}|^2 \rangle = N_{B1(B2)} \int_0^{R_0(\infty)} dr r |V_{11}^{e-i}(\mathbf{q}, r)|^2. \quad (42)$$

Equation (42) can be written as

$$\langle |[U(\mathbf{q})]_{B1(B2)}|^2 \rangle = N_{B1(B2)} R_0^2 \left[\frac{e^2}{2\epsilon_L} \right]^2 F_{B1(B2)}(q), \quad (43)$$

with form factors F_{B1} and F_{B2} for models 1 and 2, respectively. We find the analytical results,

$$F_{B1}(q) = \frac{2 \times 96^2}{(qR_0)^6} \left[[K_3(qR_0)]^2 \{ [I_0(qR_0)]^2 - [I_1(qR_0)]^2 \} + \frac{32}{(qR_0)^3} I_0(qR_0) K_3(qR_0) - \frac{8}{(qR_0)^2} \left[1 + \frac{12}{(qR_0)^2} \right] K_3(qR_0) I_1(qR_0) + \frac{64}{(qR_0)^6} + \frac{1}{(qR_0)^2} - \frac{1}{24} + \frac{(qR_0)^2}{320} \right] \quad (44a)$$

and

$$F_{B2}(q) = \frac{2 \times 96^2}{(qR_0)^6} [I_3(qR_0)]^2 \{ [K_1(qR_0)]^2 - [K_0(qR_0)]^2 \}. \quad (44b)$$

The mobility for homogeneous-background doping is expressed as

$$\mu_{B1(B2)} = \frac{\pi}{g_v} \frac{e}{\hbar} (a^*)^2 \frac{N}{N_{B1(B2)} R_0^2} \frac{[\epsilon(2k_F, T)]^2}{F_{B1(B2)}(2k_F)}. \quad (45)$$

The mobility versus electron density for model 1 is shown in Fig. 16. For charge neutrality in uncompensated semiconductors, we used $N_{B1}R_0^2/2=N$. Again, we find that local-field effects strongly reduce the mobility. The density dependence of the mobility is weaker in Fig. 16 than in Fig. 15. This is because in Fig. 16 the (one-dimensional) impurity density is set equal to the electron density.

In Figs. 15 and 16 the mobility was calculated for $T=0.02 \text{ Ry}^*$. For GaAs this corresponds to about 1 K. The Fermi energy for $N=1 \times 10^5 \text{ cm}^{-1}$ is 1 K too. We conclude that for $N > 1 \times 10^5 \text{ cm}^{-1}$ our results are consistent with the condition $T < \epsilon_F$, see Eq. (39). For $N < 10^5 \text{ cm}^{-1}$ the higher-order effects in the temperature dependence of the screening function must be considered.

D. Interface-roughness scattering

It has been shown recently that interface-roughness scattering is the dominant scattering mechanism for a two-dimensional electron gas in thin quantum wells.^{43,44} Within an infinite-barrier model the mobility for interface-roughness scattering μ_{IR} follows the law $\mu_{\text{IR}} \propto L^6$.⁴⁵ L is the width of the quantum well.

Very recently, interface-roughness (IR) scattering for quantum wires has been discussed in connection with the fluctuation of the subband energies.⁴⁶ For the derivation of the random potential for Q1D ES's, we follow the derivation for two-dimensional systems.⁹ With Eq. (1), we get

$$\langle |[U(\mathbf{q})]_{\text{IR}}|^2 \rangle = \frac{1}{m^2} \frac{\beta_{01}^4}{R_0^6} \delta^2 \eta \pi^{1/2} e^{-q^2 \eta^2 / 4} \quad (46a)$$

for interface-roughness scattering in the first subband. δ and η are the height and the range parameters of the roughness, respectively. A Gaussian-like decay of the fluctuations has been assumed.⁹ For intrasubband scattering in the higher subbands nl , β_{01}^4 in Eq. (46a) must be replaced by β_{nl}^4 , see Eq. (2). For intersubband scattering between subband nl and subband mk , β_{01}^4 in Eq. (46a)

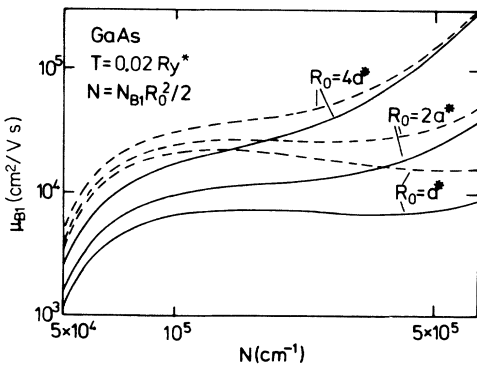


FIG. 16. Mobility for homogeneous-background doping (model 1) vs electron density for a GaAs quantum wire, see Eq. (45). The solid (dashed) lines represent calculations with (without) local-field corrections to the random-phase approximation [see Eq. (25)].

has to be replaced by $\beta_{nl}^2 \beta_{mk}^2$. The random potential can be expressed in terms of the subband energy E_{01} . With Eqs. (2) and (46a), we get

$$\langle |[U(\mathbf{q})]_{\text{IR}}|^2 \rangle = \left(\frac{dE_{01}}{dR_0} \right)^2 \eta \delta^2 \pi^{1/2} e^{-q^2 \eta^2 / 4}. \quad (46b)$$

A similar result was found for two-dimensional systems. The mobility for interface-roughness scattering is given by

$$\mu_{\text{IR}} = \frac{\pi}{g_v} \frac{e}{\hbar} (a^*)^2 \frac{1}{4\pi^{1/2} \beta_{01}^4} \frac{R_0^6 N}{\eta \delta^2 (a^*)^2} e^{k_F^2 \eta^2} [\epsilon(2k_F, T)]^2. \quad (47)$$

For small electron density ($k_F \eta \ll 1$) the mobility increases with electron density: $\mu_{\text{IR}} \approx N x [\epsilon(2k_F, T)]^2$. In the case of large electron density ($k_F \eta \gg 1$), backscattering is reduced and the mobility is strongly enhanced: $\mu_{\text{IR}} \approx \exp(k_F^2 \eta^2)$. The reduction of the backscattering was originally suggested by Sakaki¹⁵ as a possible mechanism for a strong mobility enhancement in case of remote-impurity doping. The mobility versus electron density for interface-roughness scattering is shown in Fig. 17 for various values of the range parameter for the roughness. It is clearly seen from Fig. 17 that for GaAs quantum wires one is between the above discussed limits. The density dependence of the screening function $[\epsilon(2k_F, T)]$ decreases with increasing density, see Fig. 3 of Ref. 7) is important in this regime and gives rise to a mobility which decreases weakly with increasing density. For GaAs quantum wells it was found that $\eta \approx 60 \text{ \AA}$.^{43,44} With this value for the range parameter, we find for a GaAs quantum wire the value $k_F \eta = 1$ for $N = 1.1 \times 10^6 \text{ cm}^{-1} = 2.2 N_0$. As for impurity scattering, the mobility for interface-roughness scattering is also strongly reduced if local-field corrections are taken into account, see Fig. 17.

Our calculation has been performed within the infinite-barrier approximation. With a finite-barrier model we expect that the effect of the roughness is reduced, as was found for two-dimensional systems.^{36,44} However, we find it instructive to show that the width dependence of the mobility in the infinite-barrier approximation is the same for one- and two-dimensional systems: $\mu \propto R_0^6$.

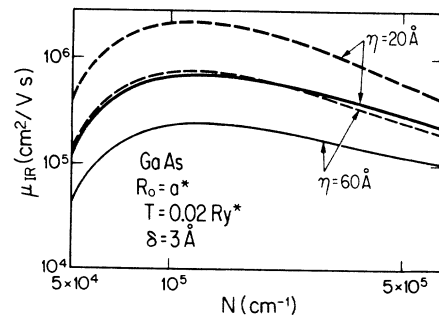


FIG. 17. Mobility for interface-roughness scattering vs electron density for a GaAs quantum wire, see Eq. (47). The solid (dashed) lines represent calculations with (without) local-field corrections to the random-phase approximation [see Eq. (25)].

VII. DISCUSSION

In this section we discuss the ground state (Fermi liquid), which we have assumed in our calculation, and the model (cylindrical wire). Some experiments on intersubband plasmons are compared with our theoretical result.

A. The ground state

From a theoretical point of view, unusual electronic properties are expected for Q1D ES's. The Peierls transition is a characteristic property of an electron-phonon system with quasi-one-dimensional electrons (for a review, see Ref. 47). Recently, the existence of a Peierls transition in Q1D ES's with long-range Coulomb interaction has been questioned.⁴⁸ Neglecting phonons, other electronic instabilities (charge-density waves, spin-density waves, and singlet and triplet superconductors) have been discussed in connection with the Tomonaga-Luttinger and Luther-Emery models (for a review, see Ref. 49). However, these models consider a short-range interaction potential. These instabilities have not been observed in artificial quantum wires.¹ Only recently have some experimental results on the density dependence of the conductance been discussed in terms of a Wigner crystal.⁵⁰

In our calculations we assume a Fermi-liquid-type behavior of the electrons. Nearly all of the experimental results¹ indicate that this assumption is adequate. However, even for a Fermi-liquid-type ground state, very different phenomena have been discussed in the literature. We mention localization effects,⁴¹ conduction fluctuations,⁵¹ and, recently, ballistic transport.⁵²

Direct experimental evidence for subbands in Q1D ES's came from transport measurements,^{52–54} capacitance measurements,⁵⁵ and infrared experiments.^{29,56–58} For a review, see Refs. 1 and 2. The infrared experiments gave evidence for intersubband plasmons, which we discussed in Sec. IV. Intracsubband plasmons in Q1D ES's have not yet been observed. The observation of intracsubband plasmons and the verification of the dispersion relation would be a strong indication for a Fermi-liquid-type ground state. Moreover, the validity of the random-phase approximation and the importance of local-field corrections could be studied.

Experimental studies on shallow impurity states in Q1D ES's have not yet been published. For such measurements the impurity position must be well defined, which is a difficult technological task. However, our theoretical results on the binding energy of shallow impurities are in agreement with variational calculations, see Sec. V.

The conductance fluctuations have been neglected in our calculation of the mobility, see Sec. VI. However, it has been shown that in multiwire systems, as used in the experiments of Refs. 29 and 56–58, the fluctuation effects average out and are less important.⁵⁹ Therefore we think that our results on the mobility could be useful for multiwire systems. Unfortunately, systematic experimental results on the mobility and the relevant scattering mecha-

nism are presently not available.

Our analytical results for the electron-impurity and electron-electron interaction potentials can be used to study other properties of Q1D ES's. In Ref. 60 the superconducting transition temperature in dirty Q1D ES's has been studied under the assumption that the electron density is constant within the wire. The authors used for the electron-electron interaction potential the analytical result originally derived in Refs. 7 and 8. Clearly, our analytical result, see Eq. (11a), is a better approximation for the electron-electron interaction potential.

B. Cylindrical wire

In the numerical work⁵ it was found that the confining potential is somehow between a harmonic-oscillator potential ($E_{\bar{n}} \propto \bar{n}$) and a square-well potential ($E_{\bar{n}} \propto \bar{n}^2$). \bar{n} is the subband index. The subband energies of the cylinder model are given by the zeros of Bessel functions, see Eq. (2). For the ten lowest subbands we get, for β_{nl} , 2.4, 3.8, 5.1, 5.5, 6.4, 7.0, 7.7, 8.4, 8.65, and 8.8. We rewrite Eq. (2) as

$$E_{\bar{n}} = E_{01}(\bar{n})^\alpha \quad \text{for } \bar{n} = 1, 2, \dots, 10. \quad (48)$$

$\alpha = 1.22$ is an averaged value. The average was performed with the 10 lowest subbands. Equation (48) is compatible with the numerical results of Ref. 5. In our model the first, fourth, and ninth subbands (for $\bar{n} < 11$) have a degeneracy of 1; all other subbands are double degenerate. Of course, all subbands have an additional spin degeneracy of 2.

We mention that a finite confining potential will reduce the subband energies in comparison to the energies in the infinite-barrier approximation. We conclude that our model is in reasonable agreement with the oscillator model used for interpretation of experiments^{29,56–58} and with numerical calculations.⁵

Our calculations are for wires with cylindrical symmetry. Shape effects of the wire cross section on the energy of hydrogenic impurity states have been found to be very small, especially if the area of the wire is kept fixed.⁶¹ For the electron-electron interaction potential we found very good agreement between results for a square wire⁶ and a cylindrical wire, see Fig. 4. For these reasons we consider shape effects not very important and we think that the wire cross section is the relevant quantity. This is certainly true for quantities for which one has to average over the wave functions: V_{ij}^{e-i} , V_{ijk}^{e-e} , Ω , E_B , and μ . The energy levels and the wave functions are certainly more sensitive to shape effects.⁵

C. Intersubband plasmons

In recent experiments^{29,56–58} the subband spacing determined from infrared measurements was found to be larger than the subband spacing determined from quantum oscillations of the magnetoresistance. It was argued that the difference is due to the depolarization of the optical resonance. In Refs. 56 and 57 the classical depolarization energy was estimated as

$$\Omega_{dc}^2 = \frac{8\pi e^2}{\epsilon_L} \frac{N}{mW^2}. \quad (49a)$$

W is the width of the one-dimensional channel. With $W^2 = \pi R_0^2$ and Eq. (4) for the subband distance we get

$$\Omega_{dc}^2 / (1 \text{ Ry}^*)^2 = 3.6Na^* [E_{21} / (1 \text{ Ry}^*)]. \quad (49b)$$

This expression exhibits the same Na^*E_{21} dependence as found in Eq. (27b). However, we got a prefactor $\frac{32}{7} = 4.57 \dots$ instead of 3.6.

We analyze the experiments^{56,57} by rewriting the equations for the depolarization shift as

$$\Omega_{dc}^2 / (1 \text{ Ry}^*)^2 = KNa^* [E_{21} / (1 \text{ Ry}^*)], \quad (50)$$

and calculate K from the intersubband plasmon energy, the subband distance, and the electron density according to Eqs. (27a) and (50). From the experiments done on InSb ($a^* = 670 \text{ \AA}$, $1 \text{ Ry}^* = 0.61 \text{ meV}$), we get, from Fig. 3 of Ref. 56, $K(N = 1.5 \times 10^6 \text{ cm}^{-1}) = 0.72$, $K(N = 2.2 \times 10^6 \text{ cm}^{-1}) = 0.63$, and $K(N = 3.0 \times 10^6 \text{ cm}^{-1}) = 0.55$. From the experiments done on GaAs ($a^* = 100 \text{ \AA}$, $1 \text{ Ry}^* = 5.3 \text{ meV}$), we get, from Fig. 3 of Ref. 57, $K(N = 3.7 \times 10^6 \text{ cm}^{-1}) = 0.68$, $K(N = 4.9 \times 10^6 \text{ cm}^{-1}) = 0.51$, and $K(N = 6.1 \times 10^6 \text{ cm}^{-1}) = 0.40$. We conclude that the experimental results on InSb and GaAs give roughly the same values for K . K decreases with increasing electron density.

The results for K from the experiment are much smaller than our theoretical prediction. In the samples used for the experiments, several subbands are occupied. Therefore we used an overly large electron density for the calculation of the experimental K . Equations (27) could also give a rough estimate for the depolarization shift for higher subbands, if the electron density of the last occupied subband is used in Eqs. (27). A calculation of K with the electron density of the last occupied subband would drastically increase the K deduced from the experiment,

and K would be in much better agreement with our prediction.

VIII. CONCLUSIONS

Analytical results for the electron-impurity and electron-electron interaction potentials and for the band bending for quasi-one-dimensional electron systems in a cylindrical semiconductor quantum wire have been presented. We have demonstrated that these analytical results are useful for the calculation of electronic properties. We discussed plasmon excitations, shallow impurity states, and mobility limits in quantum wires. Our results have been derived within the random-phase (plasmons), separable-potential (shallow impurity states), and Born approximations (mobility).

Our model calculation for cylindrical wires does not represent a very strong restriction to more general geometries. We believe that shape effects are not very important and, for the quantities discussed, the leading effects in quantum wires are determined by the area of the wire.

Owing to the absence of detailed systematic experimental results on the electronic properties of Q1D ES's quantitative comparison with experiments is presently not possible. We hope that our analytical results stimulate theoretical investigations and help to clarify future experimental results.

ACKNOWLEDGMENTS

We thank W. Hansen, P. Lee, and J. Serre for helpful discussions. This work (A. Gold) was supported by the Deutsche Forschungsgemeinschaft (Bonn, West Germany) and the U.S. Joint Services Electronics Program (Contract No. DAAL03-89-C-0001). The Groupe de Physique des Solides de l'Ecole Normale Supérieure is a Laboratoire associé au Centre National de la Recherche Scientifique (CNRS), France.

¹J. P. Kotthaus, in *Interfaces, Quantum Wells, and Superlattices*, edited by C. R. Leavens and R. Taylor (Plenum, New York, 1988), p. 95.

²F. Stern, in Ref. 1, p. 127.

³W. Y. Lai and S. Das Sarma, *Phys. Rev. B* **33**, 8874 (1986).

⁴J. A. Brum, G. Bastard, L. L. Chang, and L. Esaki, in *Proceedings of the 18th International Conference on the Physics of Semiconductors*, edited by O. Engström (World Scientific, Singapore, 1987), Vol. 1, p. 396; J. A. Brum and G. Bastard, *Superlatt. Microstruct.* **4**, 443 (1988).

⁵S. E. Laux and F. Stern, *Appl. Phys. Lett.* **49**, 91 (1986); S. E. Laux, D. F. Frank, and F. Stern, *Surf. Sci.* **196**, 101 (1988).

⁶T. Kodoma and Y. Osaka, *J. Phys. Soc. Jpn.* **55**, 3941 (1986).

⁷G. Fishman, *Phys. Rev. B* **34**, 2394 (1986).

⁸J. Lee and H. N. Spector, *J. Appl. Phys.* **57**, 366 (1985).

⁹T. Ando, A. B. Fowler, and F. Stern, *Rev. Mod. Phys.* **54**, 437 (1982).

¹⁰C. Weisbuch, in *Semiconductors and Semimetals: Application of Multiquantum Wells, Selective Doping, and Superlattices*, edited by R. Dingle (Academic, New York, 1987), Vol. 24, p. 1.

¹¹S. Das Sarma and Wu-yan Lai, *Phys. Rev. B* **32**, 1401 (1985).

¹²G. W. Bryant, *Phys. Rev. B* **29**, 6632 (1984).

¹³J. Lee and H. N. Spector, *J. Vac. Sci. Technol. B* **2**, 16 (1984).

¹⁴A. Gold, J. Serre, and A. Ghazali, *Phys. Rev. B* **37**, 4589 (1988); J. Serre, A. Ghazali, and A. Gold, *ibid.* **39**, 8499 (1989).

¹⁵H. Sakaki, *Jpn. J. Appl. Phys.* **19**, L735 (1980); *J. Vac. Sci. Technol.* **19**, 148 (1981).

¹⁶J. Lee and H. P. Spector, *J. Appl. Phys.* **54**, 3921 (1983).

¹⁷S. Flügge and H. Marschall, *Rechenmethoden der Quantentheorie*, 3rd ed. (Springer, Berlin, 1965), Problem 25.

¹⁸I. S. Gradshteyn and I. M. Ryzhik, *Table of Integrals, Series and Products* (Academic, New York, 1980).

¹⁹The correct form of Eq. (21) in Ref. 7 is $A(R < R_0) = 2[1 - \alpha K_1(\alpha)I_0(\delta)]$, with α and δ as defined in Ref. 7.

²⁰S. Das Sarma, *Phys. Rev. B* **29**, 2334 (1984).

²¹D. Pines and P. Nozières, *The Theory of Quantum Liquids* (Benjamin, New York, 1966), Vol. 1.

²²A. K. Das, *Solid State Commun.* **15**, 475 (1974).

²³P. F. Williams and A. N. Bloch, *Phys. Rev. B* **10**, 1097 (1974).

²⁴W. I. Friesen and B. Bergersen, *J. Phys. C* **13**, 6627 (1980).

- ²⁵K. S. Singwi, M. P. Tosi, R. H. Land, and A. Sjölander, *Phys. Rev.* **176**, 589 (1968).
- ²⁶B. Vinter, *Phys. Rev. B* **15**, 3947 (1977).
- ²⁷W. P. Chen, Y. J. Chen, and E. Burnstein, *Surf. Sci.* **58**, 263 (1976); S. J. Allen Jr., D. C. Tsui, and B. Vinter, *Solid State Commun.* **20**, 425 (1976).
- ²⁸Wei-ming Que and G. Kirzenow, *Phys. Rev. B* **37**, 7153 (1988); **39**, 5998 (1989).
- ²⁹W. Hansen, M. Horst, J. P. Kotthaus, U. Merkt, C. Sikorski, and K. Ploog, *Phys. Rev. Lett.* **58**, 2586 (1987).
- ³⁰R. Schwabe, A. Haufe, V. Gottschalch, and K. Unger, *Solid State Commun.* **58**, 485 (1986).
- ³¹J. A. Brum, *Solid State Commun.* **54**, 179 (1985).
- ³²G. W. Bryant, *Phys. Rev. B* **31**, 7812 (1985).
- ³³F. A. P. Osorio, M. H. Degani, and O. Hipólito, *Phys. Rev. B* **37**, 1402 (1988).
- ³⁴G. Weber, P. A. Schulz, and L. E. Oliveira, *Phys. Rev. B* **38**, 2179 (1988).
- ³⁵C. Priester, G. Allan, and M. Lannoo, *Phys. Rev. B* **29**, 3408 (1984).
- ³⁶A. Gold, *Z. Phys. B* **74**, 53 (1989).
- ³⁷O. Hipólito and V. P. Campos, *Phys. Rev. B* **19**, 3083 (1979).
- ³⁸J. A. Brum, G. Bastard, and C. Guillemot, *Phys. Rev. B* **30**, 905 (1984).
- ³⁹A. Gold and W. Götze, *Phys. Rev. B* **33**, 2495 (1986).
- ⁴⁰M. J. Rice, in *Low-Dimensional Cooperative Phenomena*, edited by H. J. Keller (Plenum, New York, 1975), p. 23.
- ⁴¹P. A. Lee and T. V. Ramakrishnan, *Rev. Mod. Phys.* **57**, 287 (1985).
- ⁴²Y. Weng and J. P. Leburton, *J. Appl. Phys.* **65**, 3089 (1989).
- ⁴³H. Sakaki, T. Noda, K. Hirakawa, M. Tanaka, and T. Matsusue, *Appl. Phys. Lett.* **51**, 1934 (1987).
- ⁴⁴R. Gottinger, A. Gold, G. Abstreiter, G. Weimann, and W. Schlapp, *Europhys. Lett.* **6**, 183 (1988).
- ⁴⁵A. Gold, *Solid State Commun.* **60**, 531 (1986); *Phys. Rev. B* **35**, 723 (1987).
- ⁴⁶H. Zarem, K. Vahala, and A. Yariv, *IEEE J. Quantum Electron.* **QE-25**, 705 (1989).
- ⁴⁷S. Kagoshima, N. Nagasawa, and T. Sambongi, *One-dimensional Conductors*, Vol. 72 of *Springer Series in Solid-State Sciences* (Springer, New York, 1988).
- ⁴⁸J. Ashkenazi, W. E. Pickett, H. Krakauer, C. S. Wang, B. M. Klein, and S. R. Chubb, *Phys. Rev. Lett.* **62**, 2016 (1989).
- ⁴⁹J. Sólyom, *Adv. Phys.* **28**, 201 (1979).
- ⁵⁰J. H. F. Scott-Thomas, S. B. Field, M. A. Castner, H. I. Smith, and D. A. Antoniadis, *Phys. Rev. Lett.* **62**, 583 (1989).
- ⁵¹Y. Imry, in *Directions in Condensed Matter Physics*, edited by G. Grinstein and G. Mazenko (World Scientific, Singapore, 1986), Vol. 1, p. 102.
- ⁵²B. J. van Wees, H. van Houten, C. W. J. Beenakker, J. G. Williamson, L. P. Kouwenhoven, D. van der Marel, and C. T. Foxon, *Phys. Rev. Lett.* **60**, 848 (1988).
- ⁵³A. C. Warren, D. A. Antoniadis, and H. I. Smith, *Phys. Rev. Lett.* **56**, 1858 (1986).
- ⁵⁴K. Ismail, D. A. Antoniadis, and H. I. Smith, *Appl. Phys. Lett.* **54**, 1130 (1989).
- ⁵⁵T. P. Smith III, H. Arnot, J. M. Hong, C. M. Knoedler, S. E. Laux, and H. Schmid, *Phys. Rev. Lett.* **59**, 2802 (1987).
- ⁵⁶J. Alsmeier, Ch. Sikorski, and U. Merkt, *Phys. Rev. B* **37**, 4314 (1988).
- ⁵⁷F. Brinkop, W. Hansen, J. P. Kotthaus, and K. Ploog, *Phys. Rev. B* **37**, 6547 (1988).
- ⁵⁸T. Demel, D. Heitmann, P. Grambow, and K. Ploog, *Phys. Rev. B* **38**, 12 732 (1988).
- ⁵⁹S. Das Sarma and X. C. Xie, *Phys. Rev. B* **35**, 9875 (1987).
- ⁶⁰H. Ebisawa, H. Fukuyama, and S. Maekawa, *J. Phys. Soc. Jpn.* **55**, 4408 (1986).
- ⁶¹G. W. Bryant, *Phys. Rev. B* **31**, 7812 (1985).